THROUGH-THE-WALL RADAR IMAGING WITH COMPRESSIVE SENSING; THEORY, PRACTICE AND FUTURE TRENDS-A REVIEW

Abdi T Abdalla

Department of Electronics and Telecommunications Engineering, College of Information and Communication Technologies,University of Dar es Salaam, P. O. Box 33335, University of Dar es Salaam.

abdit@udsm.ac.tz

ABSTRACT

Through-the-Wall Radar Imaging (TWRI) is anemerging technology which enables us to detect behind the wall targets using electromagnetic signals. TWRI has received considerable attention recently due to its diverse applications. This paper presents fundamentals, mathematical foundations and emerging applications of TWRI with special emphasis on Compressive Sensing (CS) and sparse image reconstruction.Multipath propagation stemming from the surrounding walls and nearby targets are among the impinging challenges.Multipath components produce replicas of the genuine target, ghosts, during image reconstruction which may significantly increase the probability of false alarm. The resulting ghost not only creates confusion with genuine targets but may deteriorate the performance of (CS) algorithms as described in this article. The results from a practical scenario show a promising future of the technology which can be adopted in real-life problems including rescue missions and military purposes.

INTRODUCTION

The ultimate objective of Through-the-Wall Radar Imaging (TWRI) is to sense through building walls using Electromagnetic (EM) signals to reveal targets located behind the wall. TWRI has been sought out in rescuing missions in case of fire and earthquake tragedies, in determining interior structures of inaccessible buildings, and in performing inspection for law enforcing and military applications (Setlur et al. 2013, Leigsnering et al. 2014, Abdalla et al. 2015, Leigsnering et al. 2015). This technology has witnessed a tremendous growth and attracted the attention of many researchers in the last few years.

One of the major challenges facing TWRI is multipath stemming from multiple reflections of EM waves from the walls, floors and ceilings (Chakraborty and Li 2010,Setlur et al. 2013, Leigsnering et al. 2014). During image reconstruction, multipath components of the signal give rise to replicas of genuine targets which increase the probability of false alarm. The copies of the true target, known as *ghosts*, not only populate the scene but also create confusion with genuine targets.Consequently,they jeopardize the correct target detection process leading to improper resources allocation. Recently, ghost suppression in TWRI applications became topical and has attracted the attention of many researchers.

Most of TWRI's applications entail high quality images of the scenes, which dictates the use of wide band signals, large radar apertures and effective ghost suppression method (Abdalla 2016). The high quality requirement brings the big data constraint which is currently addressed by the

application of Compressive Sensing (CS) during data acquisition and image reconstruction (Yoon and Amin 2008, Amin 2010). On the latter requirement, different multipath ghosts suppression methods have been devised including multipath exploitation-based methods with and without CS (Setlur et al. 2013, Leigsnering et al. 2014), and Aspect Dependent (AD) based methods with and without CS (Li et al. 2013, Tan et al. 2014, Abdalla et al. 2015, Guo et al 2017, Guo et al. 2018a, Guo et al. 2018b). By ghost being AD, means their locations in the image change with the radar location. Interrogating a given scene from different aspect angles results in ghost targets residing at different pixels unlike genuine targets. This peculiar property is exploited to recognize and then suppress them as in (Li et al. 2013, Tan et al. 2014, Abdalla et al. 2015, Abdalla 2016, Guo et at. 2018a).

This paper presents a brief background, mathematical formulation, and the theory behind the TWRI together with its emerging applications with a special emphasis on CS and sparse image reconstruction. To validate the concepts, real experimental data is used.In this paper, to combat the effect of multipath ghost, the AD technique based on subaperture imaging is employed.

The remainder of the paper is organized as follows: introduction on fundamentals of TWRI, the concepts of resolutions, sensitivity, dynamic range, and the signal models are also summarized. The formation of multipath ghost and their challenges are outlined. Highlights the theory behind the CS with emphasis on TWRI applications. A TWTI practical scenario is presented. Possible future works followed by conclusions.

TWRI ESSENTIALS
TWRI is rapidly growing due to its diverse applications. Currently, the research is trending on the application of CS in TWRI to improve image quality with minimum data volume. This section highlights the technical background materials needed for one to be acquainted with TWRI.

TWRI aims at sensing through building walls using RF signals to reveal targets located behind the wall. In the TWRI literature, the scene of interest is mostly interrogated using either pulsed radar or Stepped-Frequency Radar (SFR) system. In the two scenarios, the transmitted Ultra-Wide Band (UWB) signal is realized in time and frequency domains, respectively. To acquire highly resolved images using pulsed radar, the transmitted pulses should have shorter duration thereby the transmitted bandwidth increases. It is known that the Signal-to-Noise Ratio (SNR) is a function of the transmitted energy in the radar signal (Oyanet al. 2012). The energy of the pulse is specified by the transmitted peak power in the pulse and the pulse width. When transmitting shorter pulses to achieve high range resolution, it results inlow energy being transmitted and hence reduces SNR for a given transmitter power (Abdalla 2016). Thus, the radar engineers suggested alternative radar waveforms with longer time to acquire high energy with relatively good range resolution. One approach is by sequentially transmitting a series of monochromatic waves of linearly increasing frequency, known as stepped frequency signal (Abdalla 2016). Throughout this article, SFR is assumed unless stated otherwise. In the following sub-sections, the nuts and bolts of the SFR design are delineated.

Step Frequency Radar Design Parameters
In SFR, a series of M monochromatic waves whose frequencies are linearly spaced by Δf, as shown in Figure 1, are transmitted and received at each radar location with the initial frequency value f_0 and the final f_{M-1}. The number of transceivers in a physical

array or positions in Synthetic Aperture Radar(SAR) defines the aperture length of the radar system.

The choice of Δf is crucial in the SFR design as it dictates the maximum range that the radar system can unambiguously image a given scene.
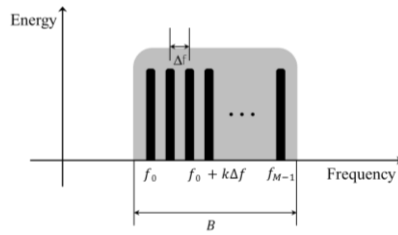

Figure 1: Step frequency signal

The maximum unambiguous range, R_{max}, is given by (Raimundo 2015, Abdalla 2016):

$$R_{max} = \frac{c}{2\Delta f} \qquad (1)$$

where c is the speed of EM wave in free space. Other important parameters in SFR design include radar resolutions, sensitivity and dynamic range.

Downrange and Crossrange Resolution

Radar resolution measures the capability of the radar to distinguish two close targets in downrange and crossrange directions (Raimundo2015, Abdalla 2016). The downrange resolution, ΔR, in meters, is the ability of the radar to resolve distinct targets positioned along the same angular displacement but at different downranges. Mathematically, ΔR is given by (Raimundo 2015, Abdalla 2016):

$$\Delta R = \frac{c}{2B} = \frac{c}{2M\Delta f} \qquad (2)$$

where B refers to the signal bandwidth.

The downrange resolution improves with increasing bandwidth and that explains why the modern TWRI systems employ UWB signals.

The crossrange resolution, ΔR_C, on the other hand, refers to the ability of the radar to distinguish adjacent targets laying at the same downrange with different angular displacements. If the SAR has aperture length, L with RF signal of wavelength, λ, and if the two targets are located at a range, $\mathbb{R}$, then the crossrange resolution is given by (Lagunas 2014, Raimundo 2015, Abdalla 2016):

$$\Delta R_C = \frac{\lambda \mathbb{R}}{2L} \qquad (3)$$

The crossrange resolution (3) improves with increasing aperture length and this explains why the modern TWRI systems use SAR to realize large apertures. The crossrange resolution is also range dependent as inferred in (3).Therefore, the farther are the targets, the lower is the crossrange resolution that the radar can achieve provided the aperture and frequency remain.

The above equation was derived for radars with narrow frequency band, monostatic configuration, and one-dimensional SAR processing. When using UWB signals, the λ varies significantly across the frequency band and, therefore, the system in such case uses upper bound instead (Abdalla 2016).

Sensitivity and Dynamic Range of the Radar

Radar sensitivity is the minimum input RF power that the radar can detect (Abdalla 2016). It provides a measure of the ability of the radar system to detect the presence of a target (Teng et al. 2007, Raimundo 2015). The dynamic range, on the other hand, is the ratio of the strongest to the weakest signal registered by the radar system and is expressed in dB(Teng et al. 2007, Raimundo 2015). This number quantifies the maximum loss that the radar signal can attain, and yet be detectable by the receiver (Abdalla 2016). TWRI may experience strong reflections from the surrounding clutters including the front wall that can limit the dynamic range

of the radar, if not properly handled. This phenomenon might saturate or even block the receiver and affect the detection of the low-cross-section targets which are treated as noise.

In the past few years, clutter mitigation was the area of interest in which the front wall clutter is mitigated prior to target detection (Yoon and Amin 2009, Tivive et al. 2011, Tivive et al. 2015). The dominant challenge in TWRI applications is the multipath components which adversely affect image reconstruction and interpretation. To better address multipath challenges and possible remedial measures, a realistic signal model is needed.

Scene Geometry and Signal Model
In TWRI, both transmitter and receiver are located on one side, a few meters from the front wall, "*stand-off distance*". EM waves traverse two different media: air and wall material, in a round trip fashion from the transmitter to the receiver. The signal undergoes a significant distortion as the wave is refracted twice, at the air-wall interface and then at the wall-air interface in the forward direction. Similar action happens as moving from the target back to the receiver (Leigsnering et al. 2014, Abdalla 2016).

When the signal reaches the target it might be reflected at one or multiple secondary reflectors leading to multipath phenomenon as shown in Figure 2. Multipath returns may result from one of the following: interior wall; floor/ceiling; wall ringing; and target-to-target interaction (Leigsnering et al. 2014, Abdalla 2016). The multipath due to the interior wall can be subdivided into first-order, second-order or higher-order multipath. In first-order multipath, only one interior wall is involved, one trip is directly from or to the target and the remaining interact with the wall to complete the trip. In second-order multipath, there are two cases:

one is similar to the previous except that the signal reflect on two interior walls and there is also a monostatic scattering scenario where transmission and reception occur along the same path but involve secondary reflectors. Whereas higher-order involves at least three secondary reflectors. Higher-order multipath are normally neglected since the received signal becomes very weak due to the additional reflections. Also the prolonged delay resulting due to multiple secondary reflections makes the target to reside outside the room during image reconstruction. (Leigsnering et al. 2014, Abdalla 2016).

In TWRI, the received signal comprises of a number of components including the front wall returns, direct returns from the targets, reflections due to the interior walls, front wall reverberations, target-to-target interactions, and floor/ceiling returns.
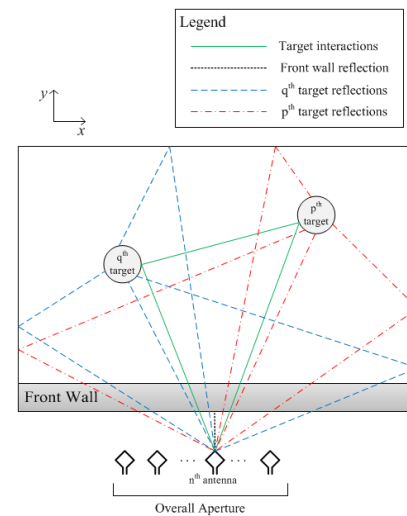

Figure 2: TWRI multipath scenario with first order returns

Interior Wall Multipath Model
Figure 3 illustrates a simple TWRI interior wall reflection scenario with only one wall to elaborate the idea. Consider a pth target located at $z_p = [x_p, y_p]^T$, and the interior

right wall parallel to the y-axis is located at $x = x_w$. Assuming specular reflection, there are two propagation paths: from the nth antenna located at x_n to the target following path-A and back to the antenna via path-B. The second is direct path without any wall reflection. It is observed that the return yields alternative antenna-target geometry and thus a virtual radar is realized located behind the same wall at $[2x_w - x_n, 0]$ simulating bistatic configuration.The delay associated with path-B is the same as that from the target to the virtual radar. This simplifies the delay calculation from the target back to the receiver as indicated bypath-B. The same principle can be readily applied to the remaining walls. The associated delay is obtained by dividing Euclidean distance by the speed of the EM wave assuming the ray tracing model.
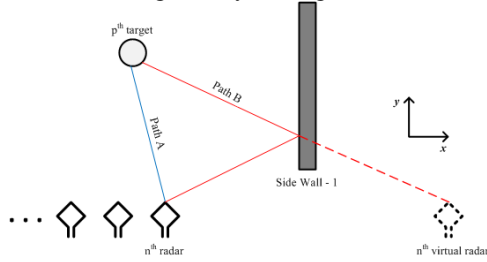

Figure 3: Multipath propagation via reflections from interior walls

Front Wall Reverberations Model
Another big challenge of TWRI is the presence of the front wall. As the wave propagates through the front wall, it gets reflected from the outer and inner surfaces of the wall causing a wall ringing or reverberation phenomenon (Karousoset al. 2008, Leigsnering et al. 2014) as depicted in Figure 4. As a result, copies of true targets are generated in the reconstructed image which are equally spaced in the radial direction from the array with exponentially reducing intensity (Leigsnering et al. 2014). These copies are termed as ghosts. The front wall returns, however, can be dealt with using available wall mitigation techniques

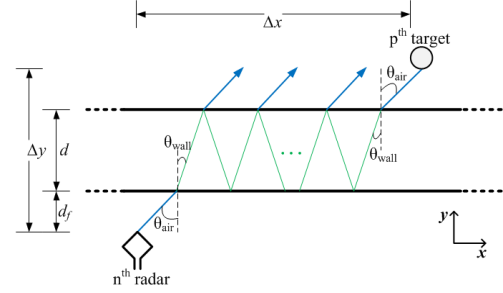(Yoon and Amin 2009, Lagunas et al. 2013, Tivive et al. 2015).

Figure 4: Wall reverberation model

Figure 4 shows the effect of wall reverberation on the transmitted signal. The distance, Δx, between the target and the array in crossrange direction is given by (Abdalla and Muqaibel 2016):

$$\Delta x = (\Delta y - d)\tan\theta_{air} + d(1 + 2k)\tan\theta_{wall} \qquad (4)$$

where Δy defines the distance between target and array element in the downrange direction, θ_{air} and θ_{wall} are the angles in the air and in the wall medium, respectively, d represents the width of the wall and k is an integer denoting the number of internal reflections. In most scenarios, the values of k do not exceed three (Ahmad and Amin 2008). The two angles are related by the famous Snell's law (Ahmad and Amin 2008):

$$\frac{\sin\theta_{air}}{\sin\theta_{wall}} = \sqrt{\varepsilon_r} \qquad (5)$$

where ε_r is the relative permittivity of the wall material. Solving the nonlinear system (4) and (5) using numerical methods gives the unknown angles. The one-way time delay that a given return will undergo due to kth wall reverberations will be (Leigsnering et al. 2014):

$$\tau(\Delta x, \Delta y, k) = \frac{(\Delta y - d)}{c\cos\theta_{air}} + \frac{d\sqrt{\varepsilon_r}(1 + 2k)}{c\cos\theta_{wall}} \qquad (6)$$

Target-to-Target Interaction

In some applications, the interaction between the targets is inevitable and therefore, the resulting returns need to be taken into consideration. As shown in Figure 2, some signal components reflect at the nearby targets as they head to the receiver. The targets interaction results in a non-linear signal component which pose computational complexity particularly when applying CS. In (Abdalla 2016), however, the author hypothesized that for two nearby and interacting targets, the overall reflectivity can be transferred to one of the target and the other target being considered as perfect reflector of a unit reflectivity. Thus, the resulting multipath will be interpreted as coming from a physical target of reflectivity equal to the product of the individuals (Abdalla 2016).

Received Signal Model
Suppose there are N radar locations and M equally spaced monochromatic waves are transmitted and received at each location to realize UWB signal(Gurbuz et al. 2009, Leigsnering et al. 2013, Muqaibel et al. 2017a). The scene is subdivided into N_x by N_y pixels along the crossrange and downrange, respectively and the target reflectivity of a pth pixel is σ_p, with $p = 0, 1, \ldots, N_x N_y - 1$. If R target returns and R_w wall returns are recorded, then the received signal at the nth radar position when the mth frequency, f_m, is $y[m,n]$, with $n = 0,1,2,\ldots, N-1$ and $m = 0,1,2,\ldots, M-1$ is given by (7)(Abdalla et al. 2015).

In (7), $t_{pn}^{(r)}$ represents the round-trip delay between the pth target and the nth receiver due to the rth return, $t_{pnq}^{(r)}$ is the round trip delay between p^{th} and q^{th} targets with n^{th} transceiver and $t_w^{(r_w)}$ is the time delay of the r_w^{th} front wall return. While $\sigma_p^{(r)}$ and $\sigma_w^{r_w}$ are the target and the wall pixel reflectivities, respectively, with respect to the rth and r_w^{th} returns, $v(m,n)$ signifies the noise sample.

The received signal comprises of four main contributions: reflection from the front wall, target-to-side wall reflection, target-to-target reflection and ambient noise.
If multipath are not well modeled, then unwanted targets will be created during image reconstruction resulting to misleading interpretation. These hypothetical, unwanted targets are known as *ghosts*.

GHOST FORMATION AND FRONT WALL MITIGATION IN TWRI
In TWRI applications, ghost targets result from interaction of the genuine targets with surrounding walls or with targets themselves. The front wall may also produce ghost when the signal suffersreverberation effect (Abdalla 2016). The ghosts due to the front wall reverberation appear in downrange direction with their spacing as a function of wall thickness and relative permittivity (Leigsnering et al. 2014, Abdalla et al. 2015). When the signal travels from the transmitter to the target, only part of it propagates straight to the target but other components get reflected by the walls, floor and ceiling before reaching the target or after being reflected back from the target to the receiver. The scattered components register different delays due to different reflecting geometries as shown in Figure 5 (a)-(c).

In such a case, the receiver interprets each of the delayed versions as they come from different physical targets which results into hypothetical targets as depicted in Figure 5 (d). The formed ghosts with the true targets fall on concentric circles with the transceiver location being their common center. The scene becomes populated and the number of expected ghosts grows proportionally with the number of true targets for a given reflecting geometry. If there are P true targets in the scene and R signal returns were recorded by the transceiver, then the number of multipath ghosts is at most

$P(R-1)$ assuming specular reflection (Abdalla 2016).

For a monostatic configuration, the possible ghost location with respect to the transceiver is estimated from the average time delay.

$$y[m,n] = \sum_{r=0}^{R-1} \sum_{p=0}^{N_x N_y - 1} \sigma_p^{(r)} \exp\left(-j2\pi f_m t_{pn}^{(r)}\right) + \sum_{r_w=0}^{R_w-1} \sigma_w^{r_w} \exp\left(-j2\pi f_m t_w^{(r_w)}\right)$$

$$+ \sum_{r=0}^{R-1} \sum_{\substack{p,q=0 \\ p \neq q}}^{N_x N_y - 1} \sigma_{pq}^{(r)} \exp\left(-j2\pi f_m t_{pqn}^{(r)}\right) + v(m,n)$$

(7)

The delay from the transmitter to the target (path-A), τ_A, and the delay from the target back to the transceiver (path-B) , τ_B, as shown in Figure 5 (a)-(c), define the average delay. The possible location of the true target is described by the circle with the radius $c\tau_A$. The locus of the ghost location due to a single bounce (first-order reflection) on the right-side wall is a circle with radius $c\left(\frac{\tau_A + \tau_B}{2}\right)$ as shown in Figure 5 (d).If the signal undergoes reflection twice at the wall (second-order reflection), the resulting ghost will reside $c\tau_B$ away from the radar as depicted in Figure 5 (d) with $\tau_B > \left(\frac{\tau_A + \tau_B}{2}\right) > \tau_A$.The left and back walls generate ghosts in a similar fashion. During SAR image reconstruction and interpretation, the formed ghost targets pose some technical challenges. However, their peculiar properties can be exploited to identify and then suppress them(Leigsnering et al. 2014, Abdalla 2016). The properties of multipath ghosts include lower crossrange resolution, non-ideal focusing and AD.

The AD property has been utilized to aid in suppressing the effect of multipath ghosts as in (Wang and Huang 2006, Tan 2010, Tan et al. 2014, Abdalla et al. 2015, Abdalla 2016).In TWRI, changing the transceiver location, alters the signal reflecting pattern and therefore, registers different values of the round-trip delays. If the scene is interrogated using different locations, their corresponding ghosts reside in different pixels while the true targets locations remain unchanged irrespective of the array shift making identification of ghost from genuine target possible. This property of the ghost is referred to as *Aspect Dependence (AD)*.

The application of CS requires the scene to be sparse which might be challenged if the front wall is not mitigated before the image reconstruction process.

Front Wall Mitigation
Without an effective wall clutter mitigation method, the targets may not be detected in the presence of strong wall reflections as the strong EM reflections obscure the targets, rendering target detection and classification difficult, if not impossible (Lagunas et al. 2013, Tivive et al. 2015, Muqaibel et al. 2017a, Tang et al. 2018). In the case of moving targets, the wall effect can be alleviated using change detection (Leigsnering et al. 2014, AlBeladi 2015). This is not possible for stationary scene, in which case the front wall reflections should be effectively attenuated before image reconstruction. In recent literatures, the common front wall mitigation techniques applied under CS framework include spatial filtering and Singular Value Decomposition

(SVD) based approaches (Lagunas et al. 2013, Tivive et al. 2015).

Spatial Filtering Based Approach

The fact that the delays of the front wall returns do not vary with the radar locations, the contribution is said to have zero spatial-
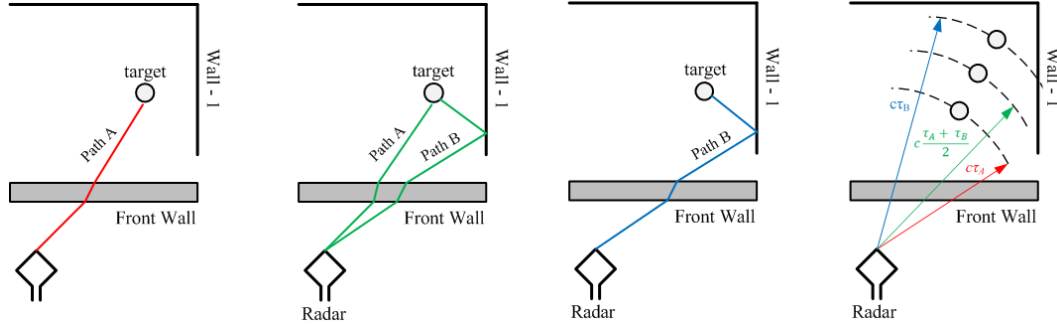

Figure 5: Some indoor multipath scenes (a) direct propagation (b) first-order interior bounce (c) second-order interior bounce (d) corresponding target and ghost locations(Abdalla 2016).

frequency. Therefore, the front wall return can be distinguished from the target returns under spatial domain. The received signal, $y[m,n]$, has, therefore, two components with regards to spatial variations. Separating front-wall contribution from target contribution amounts to basically separating a zero-frequency signal from non-zero frequency signals across antennas, which can be achieved using an appropriate spatial filter (Yoon and Amin 2009, Lagunas et al. 2013).

The spatial filter which notches out the constant component can be realized as the subtraction of the average value of the return across the array from the total return. The filtered signal, $\tilde{y}[m,n]$ is given by (Lagunas et al. 2013):

$$\tilde{y}[m,n] = y[m,n] - \frac{1}{N}\sum_{n=0}^{N-1} y[m,n] \qquad (8)$$

Singular Value DecompositionBased Approach

Alternatively, front wall mitigation under CS framework can be achieved using SVD. Suppose that the received signals are arranged into an $M \times N$ matrix, **B**(Lagunas

et al. 2013,Muqaibel et al. 2017a, Tivive et al. 2015):

$$\mathbf{B} = [\mathbf{b}_0 \mathbf{b}_1 \dots \mathbf{b}_n \dots \mathbf{b}_{N-1}] \qquad (9)$$

where $\mathbf{b}_n$ is the $M \times 1$ column vector containing the stepped frequency signal received by the nth radar given by:

$$\mathbf{b}_n = [y(0,n) \dots y(m,n) \dots y(M-1,n)]^T \qquad (10)$$

Performing SVD of **B**, gives:

$$\mathbf{B} = \mathbf{U}\mathbf{D}\mathbf{V}^H \qquad (11)$$

where $\mathbf{V}^H$ denotes the conjugate transpose of **V**, **U** and **V** are unitary matrices containing the left and right singular vectors, respectively, and **D** is a diagonal matrix containing the singular values $\lambda_1, \lambda_2, \dots \lambda_N$ in descending order. It is assumed that the front wall and target reflections lie in different subspaces. Therefore, the first K dominant singular vectors of the **B** matrix are used to construct the wall subspace $\mathbf{S}_{wall}$ (Lagunas et al. 2013):

$$\mathbf{S}_{\text{wall}} = \sum_{k=1}^{K} \boldsymbol{u}_k \boldsymbol{v}_k^H \qquad (12)$$

where $\mathbf{S}_{wall}^{\perp}$ is the subspace orthogonal to the wall subspace, given by:

$$\mathbf{S}_{\text{wall}}^{\perp} = \mathbf{I} - \mathbf{S}_{\text{wall}}\, \mathbf{S}_{\text{wall}}^{\text{H}} \qquad (13)$$

where $\mathbf{I}$ denotes the identity matrix. Now, projecting the $\mathbf{B}$-scan matrix on the orthogonal subspace, the wall returns will be mitigated, given by:

$$\widetilde{\mathbf{B}} = \mathbf{S}_{\text{wall}}^{\perp}\, \mathbf{B} \qquad (14)$$

It is shown in (Lagunas et al. 2013) that both spatial filtering and subspace methods give better results when applied under CS framework.

COMPRESSIVE SENSING

Compressive Sensing (CS) states that a sparse or compressible signal can be reconstructed using fewer measurements compared to the signal dimension contrary to conventional linear algebra theory (Candès 2006, Lagunas 2014, Masood 2015). A sparse signal refers to a signal with only few non-zero entries. While compressible signal means a signal with fewer significant entries, the remaining are not necessarily zeros (Abdalla 2016).

Many applications today with TWRI as an example, face the big data challenge. To acquire, process, and store huge amount of data using traditional techniques becomes a nightmare. In many applications though, most of the collected data is insignificant and can be dropped without compromising the quality of the expected signal (Abdalla 2016). For the past years, all this data was captured and then compressed off-line by dropping all insignificant ones. But CS provides a way to simultaneously acquire and compress the signal. This capability drastically reduces the cost and time for data acquisition and processing (Candès 2006, Donoho 2006). CS theory suggests that a signal which is not sparse or compressible in its original domain may have sparse representation in other domains (Candès 2006, Donoho 2006). Taking sinusoid signal as an example, although it is not sparse in time domain but it is in the frequency

domain. Since most of the real life scenarios including radar imaging exhibit sparsity in certain domains, CS finds itself attractive in TWRI applications as it enables significant reduction in data volumes. CS theory asserts that one can recover certain signals from far fewer samples below the Nyquist rate. To make this possible, CS relies on two principles: sparsity, which pertains to the signals of interest; and incoherence, which pertains to the sensing modality (Candès 2006).

To comprehend the idea, consider a sparse signal $\boldsymbol{s} \in \mathbb{C}^{N_x N_y \times \mathbf{1}}$ that denotes a 2D image signal of length $N_x N_y$ as presented in the previous sections. The secret behind CS reconstruction is that we acquire the measurements as linear combinations of its elements. Let $\mathbf{A} \in \mathbb{C}^{J \times N_x N_y}$ with $J \ll N_x N_y$ be a sensing matrix which defines the linear combinations of the elements of $\boldsymbol{s}$ and $\overline{\boldsymbol{y}} \in \mathbb{C}^{J \times 1}$ being the compressed measurement vector which is a linear projection of $\boldsymbol{s}$. In the presence of Gaussian noise, $\boldsymbol{v}, \overline{\boldsymbol{y}}$ can be written as (Abdalla 2016):

$$\overline{\boldsymbol{y}} = \mathbf{A}\boldsymbol{s} + \boldsymbol{v} \qquad (15)$$

A crucial stage in CS is the design of $\mathbf{A}$ to ensure that the signal information is preserved otherwise it will lead to erroneous reconstruction. If the vector of interest is not sparse in the original domain, then it can be transformed using arbitrary basis resulting in a sparse vector. Suppose, $\boldsymbol{\theta}$ is the sparse representation of $\boldsymbol{s}$ using transformation $\boldsymbol{\phi}$ such that $\boldsymbol{s} = \boldsymbol{\phi}\boldsymbol{\theta}$, the design of $\mathbf{A}$ depends very much on $\boldsymbol{\phi}$. The CS theory asserts that the columns of $\mathbf{A}\boldsymbol{\phi}$ should be as incoherent as possible to ensure correct recovery. In the literature, the performance criteria used to measure the recoverability of the given sensing matrix include but are not limited to Restricted Isometry Property (RIP), mutual coherence, spark and Null Space Property (NSP)(Leigsnering 2015). Unlike RIP, Spark and NSP are applicable only in

noiseless scenarios and, therefore, they are not suitable for TWRI applications.

Restricted Isometry Property (RIP)
A sensing matrix, **A** is said to satisfy RIP of order P if there exists a $\delta_P \in (0,1)$ such that (Candès 2006):
$$(1 - \delta_P)\|s\|_2^2 \leq \|As\|_2^2 \leq (1 + \delta_P)\|s\|_2^2 \qquad (16)$$

for all $s \in \sum_P = \{s : \|s\|_0 \leq P\}$
If equation (16) is satisfied, then this is sufficient condition for a variety of algorithms to recover a sparse signal from noisy measurements.

In TWRI applications however, RIP is quite involving even if the sparsity of the scene is known. In such cases, mutual coherence of the sensing matrix provides relatively easy alternative (Leigsnering 2015).

Mutual Coherence
In classical array literature, the array design focusses on the Point Spread Function (PSF). The normalized PSF is equivalent to the mutual coherence between columns of the sensing matrix in CS framework. The mutual coherence of a matrix **A**, $\mu(\mathbf{A})$, is the maximum absolute value of the inner product among all pairs of columns in the matrix and is given by (Donoho et al. 2012, Li et al. 2014):
$$\mu(\mathbf{A}) = \max_{i \neq j} \frac{|a_i^H a_j|}{\|a_i\|\|a_j\|} \qquad (17)$$
where a_i is the ith column vector of **A**. In classical algorithms, it may also provide useful information on the performance of the given array including resolution, robustness to noise and other interferences, and ambiguity information. When $\mu(\mathbf{A})$ is a small, it is a sufficient condition to ensure unique signal reconstruction.

Signal Reconstruction Algorithms
The traditional mathematics suggests that equation (15) has infinitely many solutions as it forms an underdetermined system. If, however, the signal is sparse, then naturally one can think of l_0-norm minimization to acquire a unique solution which is given by:
$$\tilde{s} = \text{argmin}_s \|s\|_0 \text{ s.t. } \|\bar{y} - As\|_2 < \varepsilon \qquad (18)$$
where ε is a function of noise power (Huang et al. 2010). Basically (18) counts the number of non-zero entries in a vector signal and returns the sparsest solution. This approach, though, requires exhaustive search over all possible supports of s, which is not feasible and it is therefore, labeled as *NP-hard problem* (Masood 2015).

It is reported in CS literature that such problem in (18) can be relaxed and s can be reconstructed with high probability using $J \geq CP \log\left(\frac{N_x N_y}{P}\right)$ measurements by minimizing l_1-norm (Masood, 2015):
$$\tilde{s} = \text{argmin}_s \|s\|_1 \text{ s.t. } \|y - As\|_2 < \varepsilon \qquad (19)$$

This convex optimization problem can be casted as linear program known as Basis Pursuit (BP) and number of algorithms to solve such problem are available in the literature (Abdalla 2016). BP however, are computationally inefficient particularly for large signals. To overcome this challenge, greedy algorithms, like Matching Pursuit(MP) were devised which find the support of the unknown vector iteratively (Tropp and Gilbert 2007, Needell and Vershynin 2009,Donoho et al. 2012). MP algorithm is faster but it lacksstability and also requires computation of inner products which adds complexity especially for large and less sparse vectors (Masood 2015). As a remedy, derivatives of MP have been presented that include but are not limited to Compressive Sampling Matching Pursuit (CoSAMP), Stage-wise Orthogonal Matching Pursuit (StOMP), Subspace Pursuit (SP) and Regularized Orthogonal Matching Pursuit (ROMP) as narrated in (Masood 2015).

In convex relation and greedy algorithms, the only prior information utilized is the signal sparsity. In some applications, noise statistics are available and may be used to improve signal recovery and which is the main feature of the so called Bayesian algorithms (Abdalla 2016).

Bayesian approaches attracted the attention of many researchers lately due to it superiority over conventional algorithms. Its theory had been dwelt on in (Masood 2015). In Bayesian algorithms, the unknown signal is modeled as Bernoulli-Gaussian or Bernoulli-Laplacian. If the prior statistics is assumed to follow Gaussian distribution as in many contributions, then it allows a tractable math but its feasibility is limited. The support agnostic (Masood and Al-Naffouri 2013) on the other hand, is applicable when the support distribution is not Gaussian or even unknown in priori. In TWRI applications especially when dealing with extended targets, the targets distributions are not necessarily known, which promotes the use of Bayesian algorithms.

When exploiting AD feature using multiple subapertures, the combination of subimages may be achieved using a Weighted Sum Additive–Multiplicative (WSAM) image fusion which is a two-step process. First, an intermediate image is obtained as the weighted sum of the individual subimages, s_W then the intermediate image is masked with subimage. This WSAM perform better than the conventional masking (Muqaibel et al. 2017a).

The summation preserves the magnitude of the genuine targets while attenuate those of clutters. This helps reduce the effect of the ghost and other clutters and hence increase target relative clutter peak (TRCP) at target locations.

If $\check{s}_1^{(0)}$ and $\check{s}_2^{(0)}$ represent subimages from respective subapertures, then their weighted sum is given by (Abdalla 2016):

$$s_W(p) = \alpha_1 \check{s}_1^{(0)}(p) + \alpha_2 \check{s}_2^{(0)}(p) \qquad (20)$$

where $\alpha_l \in \mathbb{R}: 0 \leq \alpha_l \leq 1$, and $l = 1,2$. The values of α_l which result in a minimum norm are obtained by solving the following optimization problem:

$$\min \left\| \alpha_1 \check{s}_1^{(0)} + \alpha_2 \check{s}_2^{(0)} \right\| \text{ subject to } \alpha_1 + \alpha_2 = 1 \qquad (21)$$

The WSAM approach is relatively immune in cases when a target of interest is not well visible from one subaperture, unlike conventional masking.

Formulation of Compressive Sensing in TWRI

The emergence of TWRI technology was an incredible milestone in the radar imaging society which enabled to capture images of the targets located behind walls. The demand of high resolution image in TWRI entails wide signal bandwidth and large aperture which consequently brings big data challenge. (Amin 2010, Leigsnering et al. 2014, Wu et al. 2014, Abdalla et al. 2015). To overcome this problem, an efficient data acqsuisition approach based on CS was first introduced in TWRI by Yoon and Amin (Yoon and Amin 2008). Their finding was a breakthrough in the research of attaining clear image while paying relatively less cost. In order to apply CS, (7) is rewritten as a linear system. The target-to-target contribution in (7) is non-linear but(Abdalla 2016) suggests that the overall signal reflectivity due to the target interactions, $\sigma_{pq}^{(r)}$ can be assumed to be dictated by the second target assuming the first target has a unity reflectivity. Then the corresponding matrix representation will be given by (Abdalla 2016).

Notationally, (23) can be written as:

$$\mathbf{y}$$
$$= \sum_{r=0}^{R-1} \mathbf{\Phi}^{(r)} \mathbf{s}^{(r)} + \sum_{r_w=0}^{R_w-1} \mathbf{\Phi}_w^{(r_w)} \mathbf{s}_w^{(r_w)} \qquad (22)$$
$$+ \sum_{r=0}^{R-1} \sum_{\substack{p,q=0 \\ p \neq q}}^{N_x N_y - 1} \mathbf{\Psi}_q^{(r)} \mathbf{s}_q^{(r)} + \mathbf{v}$$

where $\boldsymbol{s}^{(r)}$, $\boldsymbol{s}_q^{(r)}$, and $\boldsymbol{s}_w^{(r_w)} \in \mathbb{C}^{N_x N_y \times 1}$, with $r = 0, 1, \dots R - 1$ and $r_w = 0, 1, \dots R_w - 1$ represent the vectors of reflectivities, $\sigma_p^{(r)}$, $\beta_p^{(r)}$ and $\sigma_w^{r_w}$, respectively, whereas σ_p assumes a value of one if there is target at p^{th} pixel, otherwise zero.

$$
\begin{bmatrix} y[0,0] \\ y[1,0] \\ y[2,0] \\ \vdots \\ y[M-1,0] \\ y[0,1] \\ y[1,1] \\ \vdots \\ y[M-1,N-1] \end{bmatrix} =
\begin{bmatrix}
\exp\left(-j2\pi f_0 \tau_{0,0}^{(0)}\right) & \exp\left(-j2\pi f_0 \tau_{1,0}^{(0)}\right) & \cdots & \exp\left(-j2\pi f_0 \tau_{N_x N_y - 1,0}^{(0)}\right) \\
\exp\left(-j2\pi f_1 \tau_{0,0}^{(0)}\right) & \exp\left(-j2\pi f_1 \tau_{1,0}^{(0)}\right) & \ddots & \exp\left(-j2\pi f_1 \tau_{1,0}^{(0)}\right) \\
\vdots & \vdots & & \vdots \\
\exp\left(-j2\pi f_{M-1} \tau_{0,0}^{(0)}\right) & \exp\left(-j2\pi f_{M-1} \tau_{1,0}^{(0)}\right) & & \exp\left(-j2\pi f_{M-1} \tau_{N_x N_y - 1,0}^{(0)}\right) \\
\exp\left(-j2\pi f_0 \tau_{0,1}^{(0)}\right) & \exp\left(-j2\pi f_0 \tau_{1,1}^{(0)}\right) & & \exp\left(-j2\pi f_0 \tau_{N_x N_y - 1,1}^{(0)}\right) \\
\exp\left(-j2\pi f_1 \tau_{0,1}^{(0)}\right) & \exp\left(-j2\pi f_1 \tau_{1,1}^{(0)}\right) & \cdots & \exp\left(-j2\pi f_1 \tau_{N_x N_y - 1,1}^{(0)}\right) \\
\vdots & & & \vdots \\
\exp\left(-j2\pi f_{M-1} \tau_{0,N-1}^{(0)}\right) & \exp\left(-j2\pi f_{M-1} \tau_{1,N-1}^{(0)}\right) & & \exp\left(-j2\pi f_{M-1} \tau_{N_x N_y - 1,0,N-1}^{(0)}\right)
\end{bmatrix}
$$
$$
\times \begin{bmatrix} \sigma_0^{(0)} \\ \sigma_1^{(0)} \\ \sigma_2^{(0)} \\ \vdots \\ \sigma_{N_x N_y - 1}^{(0)} \end{bmatrix} + \qquad (23)
$$

The entries of the matrices $\mathbf{\Phi}^{(r)}$, $\mathbf{\Phi}_w^{(r)}$ and $\mathbf{\Psi}_q^{(r)} \in \mathbb{C}^{MN \times N_x N_y}$ are defined as (Muqaibel et al. 2017a):

$$\left[\mathbf{\Phi}^{(r)}\right]_{ip} = \exp\left(-j2\pi f_m t_{pn}^{(r)}\right) \qquad (24)$$

$$\left[\mathbf{\Psi}_q^{(r)}\right]_{ip} = \exp\left(-j2\pi f_m t_{pnq}^{(r)}\right) \qquad (25)$$

$$\left[\mathbf{\Phi}_w^{(r)}\right]_{ip} = \exp\left(-j2\pi f_m t_w^{(r)}\right) \qquad (26)$$

$$m = i \bmod M, \qquad n = \left\lfloor \frac{i}{M} \right\rfloor,$$
$$i = 0, 1, 2 \cdots MN - 1$$

From (22) the compressed measurement vector, $\bar{\mathbf{y}}$, is obtained using down-sampling matrix, **D**, and given by:

$$\bar{\mathbf{y}} = \mathbf{D}\mathbf{y} \qquad (27)$$

The sensing matrix in TWRI can be viewed as the product of two matrices, a predefined matrix which describes the signal propagation model (23) which depends on the radar parameters and the reflecting geometry. The second matrix is **D** which compresses the given measurements (Leigsnering 2015). Therefore, designing the sensing matrix in TWRI is basically designing **D**. In practice, CS is applied directly during data collection. The image vector $\boldsymbol{s}$ is then reconstructed by solving optimization problem (19) using available algorithm, given $\bar{\mathbf{y}}$. In this paper, Yall1 algorithm (Yang and Zhang 2011) is used for image reconstructions as recommended by(AlBeladi 2015). To evaluate the effectiveness of the CS in the image reconstruction, it is normally compared with the conventional DSBF algorithm.

Delay and Sum Beamforming Algorithm
For performance comparison, DSBF is used to measure the level of accuracy of the reconstructed images using CS approaches. Given a set of measurements collected from

N different transceiver locations using M monochromatic frequencies of carefully chosen band taking into account the allowable signal attenuation and practical antenna length. The complex image $I(x_p, y_p)$ of the pth grid point (x_p, y_p) is obtained by summing phase shifted copies of the received signals (Ahmad et al. 2005):

$$I(x_p, y_p) = \frac{1}{MN} \sum_{n=0}^{N-1} \sum_{m=0}^{M-1} y[m,n] \exp(j2\pi f_m \tau_{pn}) \quad (28)$$

where τ_{pn} is the focusing delay associated by the nth transceiver and the pth grid point.

Performance Metrics
To quantify the performance of the reconstructed images, three performance metrics are frequently used: Target Signal-to-Clutter Ratio (TSCR), Target Relative Clutter Peak (TRCP) and precision.

Target Signal-to-Clutter Ratio
The TSCR is defined as the ratio of the maximum target amplitude to the average amplitude in the clutter region. Mathematically, TSCR is given in logarithmic notation as (Leigsnering et al. 2014, Abdalla et al. 2015):

$$\text{TSCR} = 20 \log_{10} \frac{\max_{p \in A_t} |s(p)|}{\frac{1}{N_c} \sum_{p \in A_c} |s(p)|} \quad (29)$$

where A_t and A_c respectively denote the target and clutter areas, $s(p)$ is the signal value at corresponding the pth pixel and N_c is the number of clutter pixels. The clutter region refers to area of the room excluding the target area.

Target Relative Clutter Peak
The TRCP is the ratio of the maximum target amplitude to that of maximum clutter. It can be deduced from (29)as:

$$\text{TRCP} = 20 \log_{10} \frac{\max_{p \in A_t} |s(p)|}{\max_{p \in A_c} |s(p)|} \quad (30)$$

The TRCP is more crucial as it tells how easy the target can be distinguished from the surrounding clutters and it ,therefore, has direct consequences on the target detection than TSCR. If the TRCP is relatively small, then the probability of false alarms increases.

Precision
Similar to TRCP but more informative performance metric is the precision. Denote TP as the number of true positives and FP as false positives. The precision on the reconstructed image is given by (AlBeladi 2015):

$$\text{Precision} = \frac{TP}{TP + FP} \quad (31)$$

This metric is more suitable in evaluating the quality of the image in the presence of multipath ghosts (Abdalla 2016). In this context, when ghosts are treated as false positives or false alarms and the genuine targets as true positives, the precision gives information on the probability of correct target detection. When the precision returns the value of one, means the number of expected target was correctly reconstructed or else, the scene is contaminated with ghosts and other clutters.

Experimental validation of the technology as presented in recent literature, the above performance measures suggest that TWRI technology is capable to discern the obstructed scenes.

PRACTICAL APPLICATION OF TWRI
Using the setup presented by Figure 6 (a) and the corresponding schematic sketch of the room shown in Figure 6 (b). The images reconstructed by wideband SAR system covering 67 equally spaced locations with an inter-element spacing of 2.5cm along the x-axisare depicted in Figure 7. A stepped

frequency signal occupying a spectrum between 1 and 3GHz with 201 frequency points was used for scene interrogation which permits a range resolution of 7.5cm and maximum unambiguous range of $15m$. The background information was first captured for clutter and front wall mitigation. Two metallic cylinders used as targets were placed at $(-0.75, 2)\, m$ and $(0.5, 3)\, m$ as shown in Figure 6 (b). The center of the aperture was taken to be the system origin and the imaged region was taken to be $4 \times 5m^2$ as in (Muqaibel et al. 2017a).Figure 7 shows the images generated using DSBF with full data volume and CS using 12.5% of the data volume in Figure 7 (a) and (b), respectively.

The effect of multipath ghosts is suppressed using AD based on subaperture imaging under CS framework as presented in (Muqaibel et al. 2017a). From the measurement, only one-fourth of the frequency and one-half of the radar locations were randomly selected to sparsely reconstruct subimages as depicted in Figure 8 (a) and (b). The two subimages were then combined using WSAM fusion which shows significant ghost suppression with TSCR and TRCP of 88.0dB and 20.2dB, respectively. despite the directivity challenge of the horn antenna as depicted in Figure 8 (a) and (b)(Muqaibel et al. 2017a). This observation tells that when dealing with directional antennas, the subapertures must be carefully chosen otherwise some genuine targets might be invisible by the radar system.

The target detectability using precision was also analyzed. Precision gives a good indication of how well is the reconstruction method by comparing the expected number of targets and the number of reconstructed targets as defined in Section 3. The unit precision means the number of targets in the final image is exactly the same as the expected. The variation of the precision value with the possible threshold is given in the precision curves in Figure 8 (d).

POSSIBLE FUTURE DIRECTIONS
Multipath ghosts not only cause confusion with the genuine targets but also populate the scene rendering it less sparse which deteriorates the performance of CS. The current methods used to suppress the ghosts in TWRI literature are mostly based on post image processing. The image is firstreconstructed and then the ghosts are identified and suppressed. From CS view point, to enhance the performance of the algorithms, the effect of multipath should be suppressed prior to the image reconstruction.Further, considering the time history and moving targets are possible directions to explore.

In (Abdalla and Muqaibel 2016), the authors proposed the use of sparse arrays in TWRI applications based on primitive Pythagorean triples coprime numbers as method to suppress multipath ghost.The proposal of using Pythagorean triples in TWRI is fresh and further theoretical analysis is needed. Further research can be conducted to study the optimal configuration in 2D and propose the best arrangement for TWRI applications.
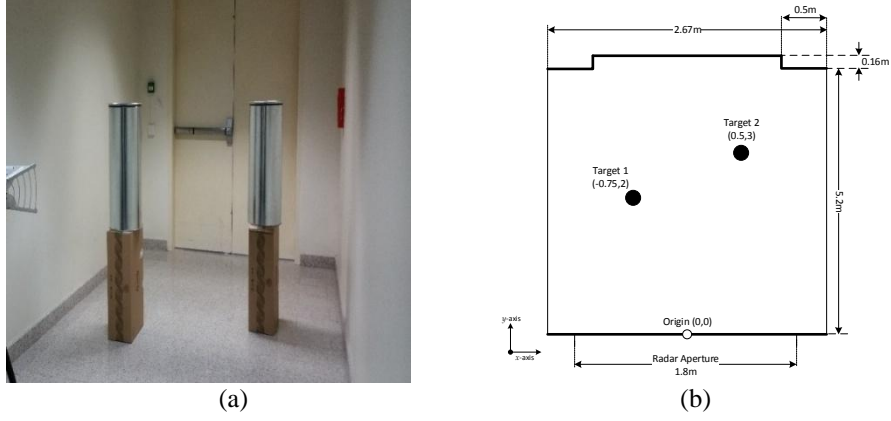
<table>
<tr><td>(a)</td><td>(b)</td></tr>
</table>

Figure 6: The scene (a) room layout (b) experimental setup (Abdalla 2016)
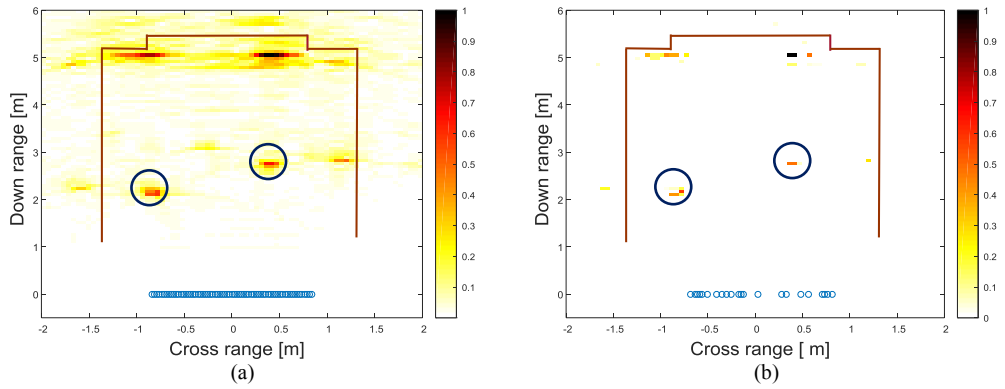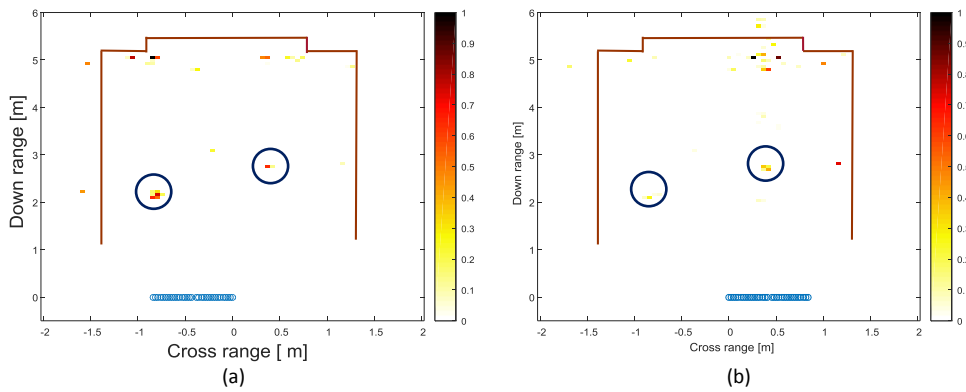

(a) (b)

Figure 7: Images (a) DSBF with full data volume (b) CS reconstruction with 12.5% data volume
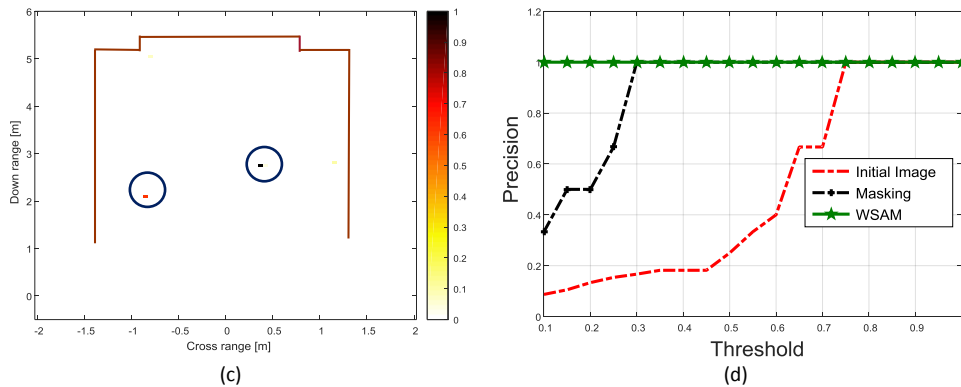

(a) (b)

Figure 8: Images (a) subaperture1 (b) subaperture2 (c) final with WSAM (d) precision

The issue of extended targets reconstruction using Block sparsity has been also pointed out in (Abdalla 2016). As the current block sparsity based methods including Block SABMP (Masood 2015) extend the block of pixels in 1D, however, based on the nature of TWRI applications, a more general algorithm which extends in 2D is required to enhance the performance.

As the concept of multipath exploitation became reality in target localization (Muqaibel et al. 2014; Muqaibel et al. 2017b), a research is also needed inTWRI to exploit multipath returns to aid in imaging in which case virtual radar locations may be used and hence the size of the physical aperture can be reduced significantly.Therefore, data acquisition time and memory demandwill be reduced dramatically.

Moreover, considering more realistic channel models that account for path-loss, antenna directivity, and target angular reflectivity are among the possible future directions.

CONCLUSIONS
TWRI particularly under CS framework, is trending and becoming more popular due to its diverse applications in social, military and medical fields. With TWRI, it is now possible to discern the obstructed scenes which may assist in security related issues in case of law enforcement or rescue missions in unexpected tragedies such as fire and earthquakes. This paper summarized the theory behind TWRI, major challenges facing the field and the sparse image reconstruction methods based on CS theory. The practical demonstrations show promising future of the field. Further, recommendations for possible research directions were also articulated.

ACKNOWLEDGEMENTS

REFERENCES
Abdalla AT 2016 *Aspect dependent efficient multipath ghost suppression in TWRI with compressive sensing*. PhD Dissertation, Department of Electrical Engineering, King Fahd University of Petroleum and Minerals.

Abdalla AT, Muqaibel AH and Al-dharrab S 2015 Aspect Dependent Multipath Ghost Suppression in TWRI under Compressive Sensing Framework. Proceedings of the Int. Conf. Comm.,

Sig. Process. and their App. (ICCSPA15). Sharjah,1–6.

Ahmad F and Amin MG 2008 Multi-location wideband synthetic aperture imaging for urban sensing applications. *Journal of the Franklin Institute*. **345**: 618–639.

Ahmad F Amin MG and Kassam S 2005 A beamforming approach to stepped-frequency synthetic aperture through-the-wall radar imaging.Proceedings of the IEEE First Int. Workshop on Comput. Adv. in Multi-Sensor Adaptive Process. Puerto Vallarta, Mexico, 24–27.

AlBeladi A 2015 *Multipath exploitation in through-the-wall radar imaging using sparsity-driven detection*. MSc Thesis, Department of Electrical Engineering, King Fahd University of Petroleum and Minerals.

Amin MG 2010,Through-the-wall radar imaging, CRC Press, Florida.

Chakraborty B and Li JZ. 2010 Multipath exploitation with adaptive waveform design for tracking in urban terrain. Proceedings of te Acoustics Speech and Signal Processing (ICASSP). Dallas, 3894–3897.

Candès EJ 2006 Compressive sampling.Proceedings of the Int. Congress of Math., Europ. Math. Society. Madrid.

Donoho DL 2006 Compressed sensing. *IEEE Trans. Info. Theory*.**52**: 1289–1306.

Donoho DL, Tsaig Y, Drori I and Starck JL 2012 Sparse solution of underdetermined systems of linear equations by stage wise orthogonal matching pursuit.*IEEE Trans. Inf. Theory*.**58**: 1094–1121.

Guo S, Guolong C, Mingyang W, Lingjiang K and Xiaobo Y 2017. Similarity-based multipath suppression algorithm for through-wall imaging radar. *IET Radar, Sonar & Navigation*.**11**: 1041–1050.

Guo S, Yang X, Cui G, Song Y and Kong L 2018a Multipath Ghost Suppression for Through-the-Wall Imaging Radar via Array Rotating. *IEEE Geoscience and Remote Sensing Letters*.**15**: 868–872.

Guo S, Cui G, Kong L and Yang X2018b An Imaging Dictionary Based Multipath Suppression Algorithm for Through-Wall Radar Imaging. *IEEE Trans. Aerospace and Elect. Systems*.**54**: 269–283.

Gurbuz A, McClellan J and Scott W 2009 A compressive sensing data acquisition and imaging method for stepped frequency GPRs.*IEEE Trans. Signal Proc*.**57**: 2640–2650.

Huang Q, Qu L, Wu B and Fang G 2010 UWB through-wall imaging based on compressive sensing.*IEEE Trans. Geosci. Remote Sens*.**48**: 1408–1415.

Karousos A, Koutitas G and Tzaras C 2008 Transmission and reflection coefficients in time-domain for a dielectric slab for UWB signals. Proceedings of the VTC Spring 2008–IEEE Vehicular Technology Conference. Singapore , 455–458.

Lagunas E 2014 *Compressive Sensing Based Candidate Detector and its Applications to Spectrum Sensing and Through-the-Wall Radar Imaging*. PhD Disseration, Department of signal theory and communications, Universitat Polit`ecnica de Catalunya.

Lagunas E, Amin MG, Ahmad F and Nájar M 2013 Wall mitigation techniques for indoor sensing within the compressive sensing framework. *IEEE Trans. Geosci. Remote Sens*.**51**: 891–906.

Leigsnering M 2015 *Sparsity-Based Multipath Exploitation for Through-the-Wall Radar Imaging*. PhD Dissertation, Elektrotechnik und Informationstechnik, Der Technischen Universitat Darmstadt.

Leigsnering M, Ahmad F, Amin M and Zoubir A 2013 Compressive sensing based specular multipath exploitation for through-the-wall radar imaging. Proceedings of the IEEE Int. Conf. Acoustics, Speech and Sig. Proces.(ICASSP). Vancouver, 6004–

6008.

Leigsnering M, Ahmad F, Amin M and Zoubir A 2014 Multipath exploitation in through-the-wall radar imaging using sparse reconstruction. *IEEE Trans. Aero. Elec. Systems*. **50**: 920–939.

Leigsnering M, Ahmed F, Amin M and Zoubir A 2015 Compressive Sensing Based Multipath Exploitation for Stationary and Moving Indoor Target Localization. *IEEE J. Selected Topics in Sig. Proc.* **9**: 1469–1483.

Leigsnering M, Amin MG, Ahmad F and Zoubir AM 2014 Multipath exploitation and suppression for SAR imaging of building interiors [An overview of recent advances]. *Sig. Proc. Magazine IEEE.* **31**: 110–119.

Li L, Boufounos P, Liu D, Mansour H, and Sahinoglu S 2014 Sparse MIMO Architectures For Through-The-Wall Imaging. Proceedings of the 8th IEEE Sensor Array and Multichannel Signal Processing Workshop (SAM). A Coruna, 513–516.

Li Z, Lingjiang K, Yong J, Zhongxing Z, and Lan F 2013A novel approach of multi-path suppression based on sub-aperture imaging in through-wall-radar imaging. Proceedings of the IEEE Radar Conference (RADAR). Ottawa, 4–7.

Masood M 2015 *Distribution Agnostic Structured Sparsity Recovery: Algorithms and Applications*. PhD Dissertation, Computer, Electrical and Mathematical Sciences and Engineering, King Abdullah University of Science and Technology.

Masood M and Al-Naffouri TY 2013 Support agnostic bayesian matching pursuit for block sparse signals. Proceedings of the 38th IEEE Int. Conf. on Acoustics, Speech and Signal Processing (ICASSP 2013). Vancouver, 4643–4647.

Muqaibel AH, Abdalla AT, Alkhodary M and Al-dharrab S 2017a Aspect dependent efficient multipath ghost suppression in TWRI with compressive sensing. *Int. J. Micro. Wireless Tech.***9**:1839-1852.

Muqaibel AH, Abdalla AT and Alkhodary M 2017b Through-the-Wall Radar Imaging Exploiting Pythagorean Coprime-Based Synthetic Apertures with Sparse Reconstruction. *J. Digital Sig. Proc.***61**: 86-96.

Muqaibel AH, Abdalla AT and Alkhodary M 2017c Indoor target localization using marginal antenna with virtual radars support. *Int. J. Micro. Wireless Tech.***9**:1863–1870.

Muqaibel AH, Amin M and Ahmad F 2014 Directional multipath exploitation for stationary target localization with a single-antenna. Proceedings of the Int. Radar Conf.: catching the invisible, Lille.

Needell D and Vershynin R 2009 Uniform uncertainty principle and signal recovery via regularized orthogonal matching pursuit. *Found. of Comp. Math.***9**: 317–334.

Oyan MJ, Hamran SE, Hanssen L, Berger T and Plettemeier D 2012 Ultrawideband Gated Step Frequency Ground-Penetrating Radar. *IEEE Trans. Geosci. Remote Sens.***50**: 212–220.

Raimundo X 2015 *FMCW Signals for Radar Imaging and Channel Sounding*. PhD Thesis, School of Engineering and Computing Sciences, Durham University.

Setlur P, Alli G and Nuzzo L 2013 Multipath exploitation in through-wall radar imaging via point spread functions. *IEEE Trans. Image Proces.* **22**: 4571–86.

Tan Q 2010 A new method for multipath interference suppression in through-the-wall UWB radar imaging. Proceedings of the 2nd Int. Conf. on Adv. Computer Control, Shenyang, 535–540.

Tan Q, Leung H, Song Y and Wang T 2014 Multipath ghost suppression for through-the-wall radar. *IEEE Trans. Aerosp. Electro. Syst.***50**: 2284–2292.

Tang VH, Bouzerdoum A and Phung

SL2018 Multipath ghost suppression for through-the-wall radar. *IEEE Trans. Aerosp. Electro. Sys.***27**: 1763–1776.

Teng Y, Griffiths H, Baker C, and Woodbridge K 2007 Netted radar sensitivity and ambiguity. *IET Radar Sonar & Navigation.***1**: 479–486.

Tivive F, Amin MG and Bouzerdoum A 2011 Wall clutter mitigation based on eigen-analysisin through-the-wall radar imaging. Proceedings of the 17th Int. Conf. DSP. Corfu, 1–8.

Tivive F, Bouzerdoum A and Amin M 2015 A Subspace Projection Approach for Wall Clutter Mitigation in Through-the-Wall Radar Imaging. *IEEE Trans. Geosci. Remote Sens.* **53**: 2108–2122.

Tropp J and Gilbert A 2007 Signal recovery from random measurements via orthogonal matching pursuit. *IEEE Trans. Inf. Theory.***53**: 4655–4666.

Wang L, & Huang, X. 2006. Research on UWB SAR Image Formation with Suppressing Multipath Ghosts. Proceedings of the CIE Int. Conf.

Radar.Shanghai, 1–3.

Wu Q, Zhang YD, Amin MG, and Ahmad F 2014 Through-the-wall radar imaging based on modified Bayesian compressive sensing. Preceedings of the IEEE China Summit & Int. Conf. Signal and Info. Proc. Xian, 232–236.

Yoon YS and Amin M 2008 High resolution through-the-wall radar imaging using extended target model. Proceedings of the IEEE Radar Conf. Rome, 1–4.

Yang J and Zhang Y 2011 Alternating direction algorithms for L1-problems in compressive sensing. *SIAM J. Scient. Comp.***33**: 250–278.

Yoon YS and Amin M 2008 Compressed sensing technique for high-resolution radar imaging. Proceedings of SPIE Signal Processing, Sensor Fusion and Target Recognition XVII.Florida.

Yoon YS and Amin, M. 2009 Spatial filtering for wall-clutter mitigation in through-the-wall radar imaging. *IEEE Trans. Geosci. Remote Sens.* **47**: 3192–3208.